CROATICA CHEMICA ACTA CCACAA **69** (1) 223–239 (1996)

ISSN-0011-1643
CCA-2299 *Original Scientific Paper*

Formation of ZrO_2 by the Thermal Decomposition of Zirconium Salts

Goran Štefanić,[a] *Svetozar Musić,*[a] *Stanko Popović,*[a,b] *and Krešimir Furić*[a]

[a]*Ruđer Bošković Institute, P. O. Box 1016, 10001 Zagreb, Croatia*

[b]*Department of Physics, Faculty of Science University of Zagreb, P. O. Box 162, 10001 Zagreb, Croatia*

Received May 31, 1995; revised July 14, 1995; accepted August 25, 1995

Hydrated zirconium salts containing Cl^-, NO_3^- or SO_4^{2-} anions were thermally treated up to 1300 °C. The thermal decomposition products were investigated using the X-ray diffraction (XRD), Fourier transform IR spectroscopy (FT-IR) and laser Raman spectroscopy. The thermal decomposition products of all three zirconium salts, characterized as amorphous material, showed a maximum of X-ray scattering at ~16° and also in the corresponding FT-IR spectra a broad band at 450 cm^{-1}. With an increase of the heating temperature of all three salts (400 °C for $ZrOCl_2 \cdot 8H_2O$, 400 °C for $ZrO(NO_3)_2 \cdot 2H_2O$ and 700 °C for $Zr(SO_4)_2 \cdot 4H_2O$), the metastable *t*-ZrO_2 was formed, which disappeared on further heating to higher temperatures. The yield of *t*-ZrO_2, measured by XRD, depended on the nature of the starting salt, and the highest value was obtained for $ZrOCl_2 \cdot 8H_2O$ salt. The *t*-ZrO_2 phase formed from $ZrOCl_2 \cdot 8H_2O$ was thermally most unstable, while the presence of a small amount of *t*-ZrO_2 was observed in the thermal decomposition product obtained by heating $Zr(SO_4)_2 \cdot 4H_2O$ even at 1300 °C. Metastable *t*-ZrO_2, generated by the thermal decomposition of $ZrOCl_2 \cdot 8H_2O$ or $ZrO(NO_3)_2 \cdot 2H_2O$ salt, was highly sensitive to mechanical treatment, while metastable *t*-ZrO_2 formed from $Zr(SO_4)_2 \cdot 4H_2O$ was stable during the same process. The nature of the starting salt influenced the formation of metastable *t*-ZrO_2; however, when *t*-ZrO_2 was once formed, its stability depended on the anionic impurities that remained in the oxide material.

INTRODUCTION

Zirconia, ZrO_2, is a very important material in the production of different technical ceramics. Also, zirconia can be used as a solid electrolyte in oxygen sensors, fuel cells, *etc.* Pure zirconia melts at an extremely high temperature, and it is characterized by three polymorphs, monoclinic (*m*), tetragonal (*t*) and cubic (*c*), which undergo phase transition as follows:

$$\text{melt} \xrightarrow{2680\,^\circ C} \text{cubic} \xrightarrow{2370\,^\circ C} \text{tetragonal} \underset{1170\,^\circ C}{\overset{850-1000\,^\circ C}{\rightleftharpoons}} \text{monoclinic}$$

Formation of ZrO_2 polymorphs depends on the nature of the precursor and the history of the thermal treatment. At room temperature (RT), pure zirconia is monoclinic, having a distorted fluorite-type (CaF_2) structure, with the Zr atom in the coordination seven. In both high-temperature phases, the Zr atom assumes coordination eight, as in CaF_2, but in tetragonal form the O atom is displaced from its ideal position $\frac{1}{4}$, $\frac{1}{4}$, $\frac{1}{4}$. The tetragonal and cubic polymorphs of zirconia can be stabilized at RT by addition of suitable oxides, viz. MgO, CaO, Sc_2O_3, Y_2O_3 and certain lanthanoid oxides. Crystal data for zirconia polymorphs, based on literature data, are given in Table I.[1-3] An or-

TABLE I

Polymorphs of ZrO_2

Polymorph	Space group	Z	Unit-cell parameters (Å)	t (°C)	Reference
monoclinic ZrO_2	$P2_1/c$	4	$a = 5.1505(1)$, $b = 5.2116(1)$, $c = 5.3173(1)$, $\beta = 99.230(1)°$	RT	1.
monoclinic ZrO_2	$P2_1/a$	4	$a = 5.3129$, $b = 5.2125$, $c = 5.1471$, $\beta = 99.218°$	25.5	2. PDF 37-1484
monoclinic ZrO_2	$P2_1/c$	4	$a = 5.1463$, $b = 5.2135$, $c = 5.3110$, $\beta = 99.2°$	RT	2. PDF 36-420
tetragonal ZrO_2	$P4_2/nmc$	2	$a = 3.64$, $c = 5.27$	1250	3.
*tetragonal ZrO_2	$P4_2/nmc$	2	$a = 3.6055(1)$, $c = 5.1797$	RT	1.
**cubic ZrO_2	$Fm3m$	4	$a = 5.0858(1)$	RT	1.

* = exact formula $Zr_{0.935}Y_{0.065}O_{1.968}$
** = exact formula $Zr_{0.875}Mg_{0.125}O_{1.875}$

thorhombic form has also been prepared by quenching from high pressure and temperature.[1] Because of its high melting point, zirconia is an attractive refractory material. However, the anisotropic thermal expansion behaviour of the monoclinic and tetragonal phases causes crumbling of zirconia ceramics on cooling from the sintering temperature. The tetragonal-monoclinic transition of zirconia exhibits many of the characteristics typical of the martensitic transition in metals. This fact can be exploited to toughen zirconia ceramics, as well as other ceramics, *e.g.* alumina containing zirconia. The toughening process depends upon the size and shape of particles and the stabilizing oxide phase concentration.

The first report on the existence of low temperature t-ZrO_2 was given by Clark and Reynolds.[4] At present, it is well known that metastable t-ZrO_2 can be obtained by different ways from zirconium salts or from amorphous zirconium hydroxide. However, there are still some discrepancies concerning the structure of amorphous zirconia precursor, as well as of the mechanism of zirconia polymorph transitions. Garvie[5,6] suggested the existence of a low temperature tetragonal phase as a result of lower surface energy of the tetragonal phase as compared with that of the monoclinic phase. The experimental results obtained by ball-milling at ambient conditions supported this hypothesis. When the grinding of the starting material sufficiently decreased the crystallite size, the $m \rightarrow t$ transition occurred.[7] In the bulk material, this transition normally occurred at 1170 °C. In milled samples, impurities also affected the phase transition $m \rightarrow t$. The stabilizing influence of impurities on the existence of low temperature t-ZrO_2 was examined by several researchers.[8–11] Mitsuhashi *et al.*[12] extended the theory of Garvie by introducing the lattice strain. They found that strain-free single-domain tetragonal particles transformed much easier than polydomain particles with large strains. On the basis of radial distribution functions obtained by X-ray and neutron diffraction, Livage *et al.*[13] found that the amorphous ZrO_2 precursor possessed some structural features observed in tetragonal zirconia. This result was confirmed by Raman scattering.[14] Tani *et al.*[15] prepared hydrothermally t-ZrO_2, having ultrafine particles, from the amorphous hydrous zirconia precursor. It was suggested that t-ZrO_2, under hydrothermal conditions, crystallized topotactically on the nuclei in the amorphous hydrous zirconia with structural features similar to t-ZrO_2. The effect of water vapour on the crystallite growth and the ZrO_2 transition, $t \rightarrow m$, were investigated[16] during the thermal decomposition of differently prepared ZrO_2 powders up to 1000 °C. Water vapour markedly accelerated crystallite growth of both m- and t-ZrO_2 and facilitated the transition, $t \rightarrow m$. Thermal decomposition of the amorphous zirconia precursor, which can be described with the formula $ZrO_{2-x}(OH)_{2x} \cdot yH_2O$, $x \leq 2$, $y \cong 1$, showed the amorphous nature of the precipitate up to 400 °C.[17] At 500 °C, the transition of the amorphous zirconia precursor to either the metastable t- or m-phase depended on the x value. Murase and Kato[18] examined the transition of tetragonal ZrO_2 by ball-milling in different atmospheres. They established

the important role of water adsorption on the surface of the particles for the $t \rightarrow m$ transition of the milled samples.

Davis[19] found that the pH of the precipitated amorphous ZrO_2 precursor affected the phase composition of its calcination products at 600 °C. The *m*-ZrO_2 was prepared from the precursor precipitated in the 6.5 to 10.4 pH range, while the *t*-ZrO_2 was obtained from precursors precipitated in the 3 to 4 or 13 to 14 pH range. Amorphous ZrO_2 precursor precipitated at 2.95 was calcined at 500 °C for various time intervals.[20] For prolonged times of calcination, the $t \rightarrow m$ transition was observed, and it was concluded that this transition did not occur due to a critical particle size effect. Srinivasan *et al.*[21] observed that addition of NH_4OH to $ZrCl_4$ solution at pH 10.5 affected the phase composition of the calcination products of the amorphous ZrO_2 precursor. Mamott *et al.*[22] observed the effect of pH, attained in precipitation of the amorphous ZrO_2 precursor, on the composition of calcination products, as well as on the transition $t \rightarrow m$. They suggested that amorphous zirconia retained some structural features of the parent $ZrOCl_2 \cdot 8H_2O$ salt. The effect of lattice defects on stabilization of metastable *t*-ZrO_2 was investigated by Torralvo *et al.*[23] Osendi *et al.*[24] investigated formation of metastable *t*-ZrO_2 by the thermal decomposition of the amorphous ZrO_2 precursor or zirconyl acetate, and they suggested that, initially, nucleation of *t*-ZrO_2 was favoured by creation of anionic vacancies with trapped electrons. At high temperatures, the electronic defects disappeared, the crystallites grew and nucleation of *m*-ZrO_2 phase took place. The existence of low temperature *t*-ZrO_2 in a mixture with *m*-ZrO_2 was suggested on the basis of investigations of the thermal decomposition of $ZrOCl_2 \cdot 8H_2O$.[4,9,25]

Formation of ZrO_2 by the thermal decomposition of zirconium salts was surprisingly little investigated in relation to wet chemical procedures, followed by thermal treatment of amorphous or slightly crystalline ZrO_2 precursors. The aim of the present work was to examine the thermal decomposition of zirconium salts containing Cl^-, NO_3^- or SO_4^{2-} anion and also to ascertain differences in their thermal and mechanical behaviour. Chemical and structural changes in the solids were monitored by X-ray powder diffraction, Fourier transform infrared spectroscopy and laser Raman spectroscopy.

EXPERIMENTAL

Chemicals: $ZrOCl_2 \cdot 8H_2O$ (abbreviated as ZC) obtained by Merck, $ZrO(NO_3)_2 \cdot 2H_2O$ (abbreviated as ZN) obtained by Ventron and $Zr(SO_4)_2 \cdot 4H_2O$ (abbreviated as ZS) obtained by Hopkins & Williams Ltd. were used. These chemicals were heated in air for different times. Experimental conditions for the thermal decomposition of zirconium salts and notation of the samples are given in Table II.

X-ray powder diffraction (XRD) measurements were performed at RT using a Philips counter diffractometer MPD1880 with monochromatized Cu$K\alpha$ radiation (graphite monochromator).

TABLE II

Time (hours) of the thermal treatment of zirconium salts at different temperatures ($ZrOCl_2 \cdot 8H_2O$=ZC, $ZrO(NO_3)_2 \cdot 2H_2O$=ZN, $Zr(SO_4)_2 \cdot 4H_2O$=ZS)

Sample	t (°C)								
	100	200	300	400	500	600	700	900	1300
ZC									
ZC300	2	2	2						
ZC400	2	2	2	2					
ZC500	2	2	2	2	2				
ZC700	2	2	2	2	2		2		
ZC900	2	2	2	2	2		2	2	
ZC1300	2	2	2	2	2		2	2	2
ZN									
ZN300	2	2	2						
ZN400	2	2	2	2					
ZN500	2	2	2	2	2				
ZN700	2	2	2	2	2		2		
ZN900	2	2	2	2	2		2	2	
ZN1300	2	2	2	2	2		2	2	2
ZS									
ZS200	2	2							
ZS300	2	2	2						
ZS400	2	2	2	2					
ZS500	2	2	2	2	2				
ZS600	2	2	2	2	2	2			
ZS700	2	2	2	2	2	2	2		
ZS900	2	2	2	2	2	2	2	2	
ZS1300	2	2	2	2	2	2	2	2	2

FT-IR spectra were recorded at RT using a Perkin-Elmer spectrometer, model 2000. The FT-IR spectrometer was coupled to a personal computer loaded with the IR Data Manager (IRDM) program. The specimens in powder form, used for FT-IR measurements, were prepared using the following methods: (*a*) the samples were slightly pressed by hand on the polyethylene foil surface; (*b*) the samples were ground in agate mortar and pressed by Carver press in tablets under a pressure of 500 MPa. The obtained tablets were ground into powder and slightly pressed by hand on the polyethylene foil surface. Spectra recorded in the mid infrared region were merged at 600 cm^{-1} with the spectra recorded in the far infrared region. For this purpose, a specially written computer program was used.

Raman spectra were recorded using a DILOR Z24 triple monochromater with a 514.5 nm line of COHERENT INNOVA-100 argon laser as excitation source. A spinning cell and the multiscanning technique had to be used. Specimens were prepared

for the laser Raman spectroscopic measurement using the following methods: (*c*) samples were grounded with spectroscopically pure KBr in agate mortar and then pressed into tablets under a pressure of 500 MPa and (*d*) glass capillary tubes were filled with powdered samples.

The purpose of using different procedures in sample preparation was to investigate their influence on the t-$ZrO_2 \rightarrow m$-ZrO_2 transition.

RESULTS AND DISCUSSION

X-ray diffraction

In the present work, m-ZrO_2 and t-ZrO_2 were identified by XRD according to the data in the ICCD Powder Diffraction File[2] (cards 37–1484, 36–420, 24–1164). The same File was also used for the identification of the starting Zr-salts (8–495 for ZS, 22–1022 for ZN, 32-1498 for ZC). The values of interplanar spacing and the related diffraction intensities, found in the present work, were in very good agreement with those in the ICCD PDF card no. 37-1484; therefore, these values were used for calibration of the angular scale of the diffractometer. The volume fractions of m-ZrO_2 and t-ZrO_2 were found by measuring integrated intensities of monoclinic $\bar{1}11$ and 111, as well as tetragonal 101 diffraction lines following the procedure proposed by Toraya *et al.*[26] Volume fractions are given by equations:

$$\upsilon_m = \frac{1.311\,x}{1 + 0.311\,x}, \quad \upsilon_t = 1 - \upsilon_m, \quad x = \frac{Im(\bar{1}11) + Im(111)}{Im(\bar{1}11) + Im(111) + It(101)}$$

In the cases where the samples showed a pronounced broadening of diffraction lines, the crystallite size was estimated using the Scherrer equation

$$D = \frac{0.9\,\lambda}{\beta \cdot \cos\theta}$$

λ being the X-ray wavelength, θ the Bragg angle, β pure full width at one half of maximum intensity. The pure widths were found from the observed width, after correction for instrumental broadening, for which the corresponding widths of the samples heated at 1300 °C were used, following the procedure given in literature.[27] Results of the XRD phase analysis are summarized in Table III, with the volume fractions of m-ZrO_2 and t-ZrO_2 indicated, as well as the extent of diffraction line broadening. Characteristic parts of X-ray diffraction patterns of selected samples are shown in Figures 1, 2 and 3. Table III shows that the m-ZrO_2 fraction increases and t-ZrO_2 fraction decreases with increased heat treatment temperature. In contrast

TABLE III

X-ray powder diffraction phase analysis of the samples obtained by the thermal decomposition of zirconium salts

Sample	Phase composition (approx. volume fraction)	Remark
ZC	$ZrOCl_2 \cdot 8H_2O$	SDL
ZC300	amorphous	
ZC400	t-ZrO_2 (0.97) + m-ZrO_2(0.03)	BDL
ZC700	m-ZrO_2 (0.96) + t-ZrO_2 (0.04)	LBDL
ZC1300	m-ZrO_2	SDL
ZN	$ZrO(NO_3)_2 \cdot 2H_2O$	SDL
ZN300	amorphous	
ZN400	m-ZrO_2 (0.51) + t-ZrO_2 (0.49)	VBDL
ZN500	m-ZrO_2 (0.62) + t-ZrO_2 (0.38)	VBDL
ZN700	m-ZrO_2 (0.95) + t-ZrO_2 (0.05)	BDL
ZN1300	m-ZrO_2	SDL
ZS	$ZrO(SO_4)_2 \cdot 4H_2O$	gradual slow decrease of
ZS200	ZS	peak intensities and increase of
ZS300	ZS	broadening of diffraction lines
ZS600	amorphous + ZS (traces)	
ZS700	m-ZrO_2 (0.77) + t-ZrO_2 (0.23)	BDL
ZS1300	m-ZrO_2 (0.97) + t-ZrO_2 (0.03)	LBDL

Descriptions: SDL = sharp diffraction lines, LBDL = slightly broadened diffraction lines, BDL = broadened diffraction lines, VBDL = very broadened diffraction lines

to the results of Ravelle-Chapuis *et al.*[25], we did not observe that the t-ZrO_2 fraction increased with increasing the temperature from 400 °C to 500 °C. The samples prepared from chloride and nitrate salts at 1300 °C contained m-ZrO_2 as a single phase, while the samples obtained from sulfate salt at 1300 °C contained a small fraction of t-ZrO_2. The diffraction line broadening decreases as the heat treatment temperature of the samples increases. Table III. also indicates that the transition mechanism of zirconium salts to zirconium oxide phases involves amorphous phase as precursor of the oxide phase. The XRD analysis points to the conclusion that the stability of zirconium salts increases in the order of their anions $Cl^- \rightarrow NO_3^- \rightarrow SO_4^{2-}$ in the case of thermal decomposition of these salts.

The unit cell parameters of m-ZrO_2 at RT (25 °C), with the axes orientation corresponding to the space group $P2_1/a$, were found to be a=5.313(1) Å, b=5.213(1) Å, c=5.148(1) Å, β=99.22(2)°. The tetragonal phase, t-ZrO_2, exhibited a small number of rather broadened diffraction lines. Its unit-cell parameters at 25 °C, calculated from the diffraction pattern of sample ZC400 and

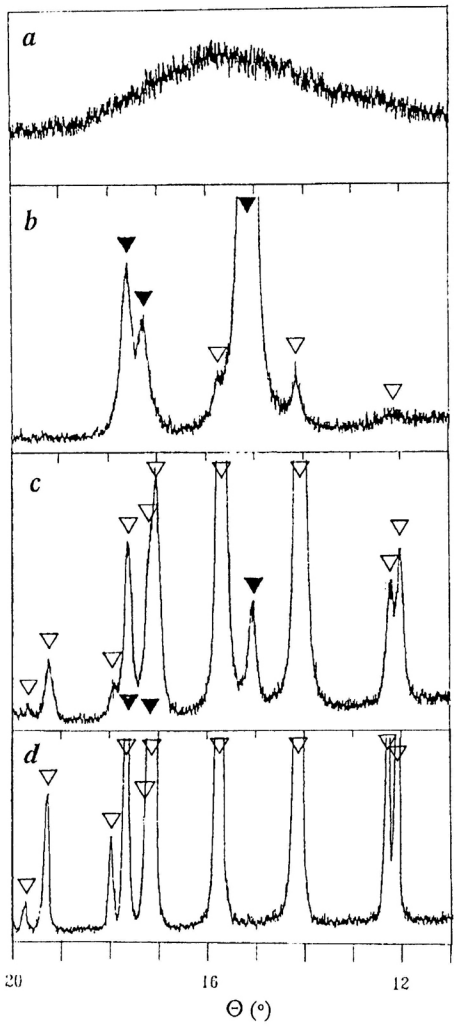

Figure 1. Characteristic parts of X-ray diffraction patterns of the samples recorded at 25 °C: (a) ZC300, (b) ZC400, (c) ZC700 and (d) ZC1300 (radiation: Cu$K\alpha$). Descriptions: ▼ = t-ZrO_2, ▽ = m-ZrO_2.

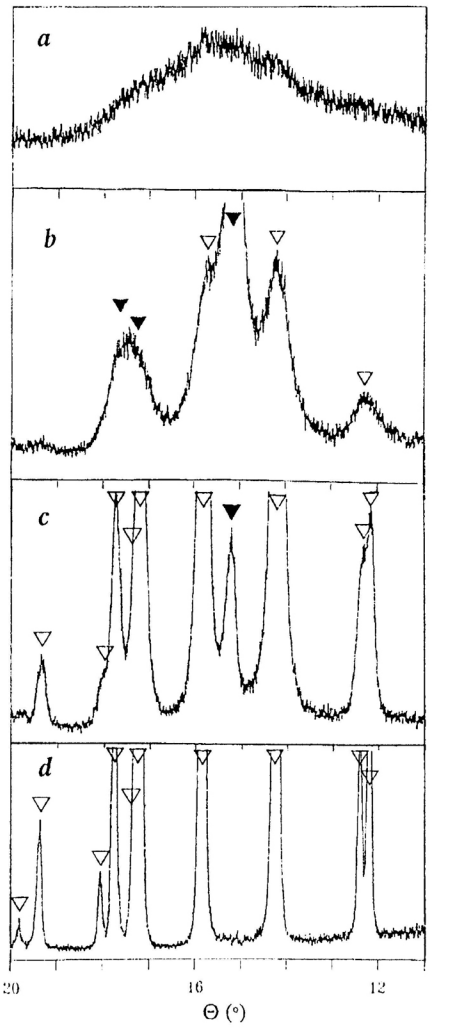

Figure 2. Characteristic parts of X-ray diffraction patterns of the samples recorded at 25 °C: (a) ZN300, (b) ZN400, (c) ZN700 and (d) ZN1300 (radiation: Cu$K\alpha$). Descriptions: ▼ = t-ZrO_2, ▽ = m-ZrO_2.

using diffraction lines of m-ZrO_2 as internal standard, are a=3.612(5) Å, b=5.192(5) Å. The samples prepared from zirconyl nitrate and heated up to ~700 °C exhibited a pronounced diffraction broadening. The estimated crystal-

lite sizes were 65 Å for sample ZN400, 95 Å for sample ZN500 and 300 Å for sample ZN700, supposing that no strain broadening was present.

FT-IR spectroscopy

The results of FT-IR spectroscopic measurements obtained by method (*a*), described in the Experimental, are summarized in Figures 4, 5, 6 and 7. The FT-IR spectrum of $ZrOCl_2 \cdot 8H_2O$, shown in Figure 4, is characterized by a strong and broad band with transmittance minimum at 478 cm^{-1}. In the same IR region, weak peaks at 584, 535 and 448 cm^{-1}, and shoulders at 419 and 328 cm^{-1} are visible. Two weak IR bands are located at 283 and 251 cm^{-1}. In the far infrared region, medium intensity bands with transmittance minimum at 193 and 178 cm^{-1} are also visible. Heating of $ZrOCl_2 \cdot 8H_2O$ at 300 °C caused changes in the corresponding FT-IR spectrum. A strong and broad IR band with transmittance minimum at 450 cm^{-1} and shoulders at 535, 328 and 193 cm^{-1} are formed. Evidently, sample ZC300 which was amorphous material for XRD, can be considered a precursor of the crystalline ZrO_2 phases. With further increase of the heating temperature, the following changes in FT-IR spectra are observed. In the spectrum of sample ZC400, new weak bands at 373-351 and 265 cm^{-1} appeared and the strong band transmittance minimum was shifted from 450 to 495 cm^{-1}. Also, the shoulder at 193 cm^{-1}, observed in the FT-IR spectrum of sample ZC300, became a well pronounced and broad band with shoulders at 228 and 176 cm^{-1}. The spectrum of sample ZC400 can be ascribed[30] to *t*-ZrO_2; however, the appearance of the weak IR band at 265 cm^{-1} and the shoulder at 228 cm^{-1} also indicate a small amount of *m*-ZrO_2 in the same sample, which is in agreement with XRD measurements. The FT-IR spectra, recorded for the samples produced at higher temperatures, up to 1300 °C, indicate evolution to the spectrum of *m*-ZrO_2.

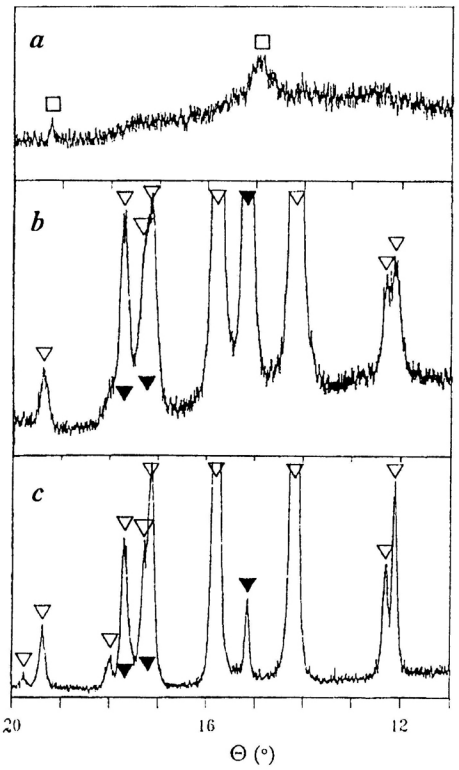

Figure 3. Characteristic parts of X-ray diffraction patterns of the samples recorded at 25 °C: (a) ZS600, (b) ZS700 and (c) ZS1300 (radiation: Cu*K*α). Descriptions: ▼ = t-ZrO_2, ▽ = m-ZrO_2, □ = $Zr(SO_4)_24H_2O$.

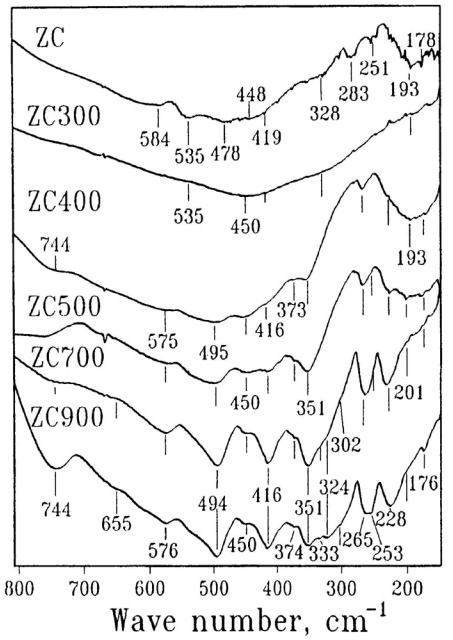

Figure 4. FT-IR spectra of samples: ZC = $ZrOCl_2 \cdot 8H_2O$, ZC300, ZC400, ZC500, ZC700 and ZC900. The specimen for the FT-IR measurement was prepared by method (a), as described in Experimental.

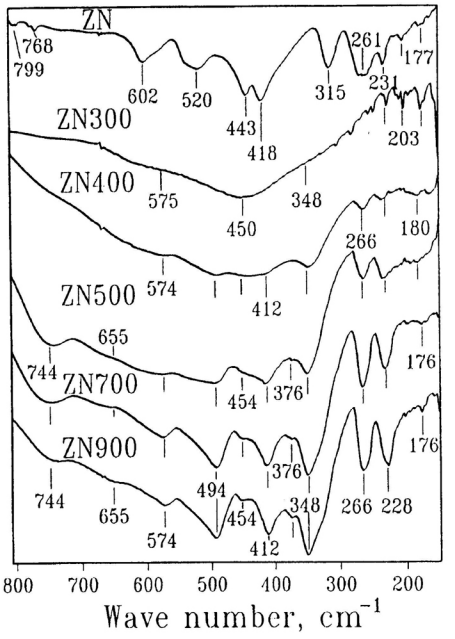

Figure 5. FT-IR spectra of samples: ZN = $ZrO(NO_2)_2 \cdot 2H_2O$, ZN300, ZN400, ZN500, ZN700 and ZN900. The specimen for the FT-IR measurement was prepared by method (a), as described in Experimental.

FT-IR spectra, shown in Figure 5, show spectral changes resulting from heating $ZrO(NO_3)_2 \cdot 2H_2O$ up to 900 °C. The spectrum of the sample heated at 300 °C shows, similarly to the case of chloride salt, formation of a broad band with transmittance minimum at 450 cm^{-1} and shoulders at 575 and 348 cm^{-1}. XRD shows the amorphous nature of this sample. The relative intensities of the bands at 266 and 228 cm^{-1}, observed for sample ZN400, gradually increase with an increase of heating temperature, thus indicating the increase of the *m*-ZrO_2 fraction. Traces of nitrate groups were still observed in sample ZN700.

FT-IR spectra, shown in Figure 6, indicate the stability of hydrated zirconium sulfate upon the thermal treatment. Spectra of samples ZS200, ZS300 and ZS500 show the main features of the starting zirconium salt. The spectrum of sample ZS600 shows a broad band at 450 cm^{-1} which can be ascribed to the amorphous fraction in this sample. Weak bands at 655, 625 and 591 cm^{-1} indicate the traces of the original salt which is in agreement with XRD. The presence of small bands characteristic of sulfate anion was detected even for sample ZS1300.

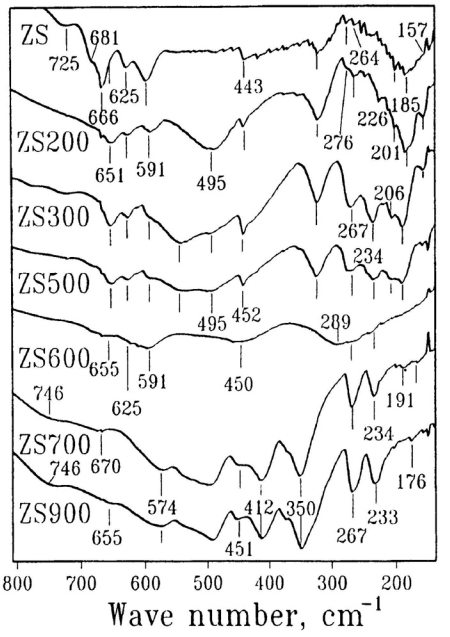

Figure 6. FT-IR spectra of samples: ZS = $Zr(SO_4)_2 \cdot 4H_2O$, ZS200, ZS300, ZS500, ZS600, ZS700 and ZS900. The specimen for the FT-IR measurement was prepared by method (a), as described in Experimental.

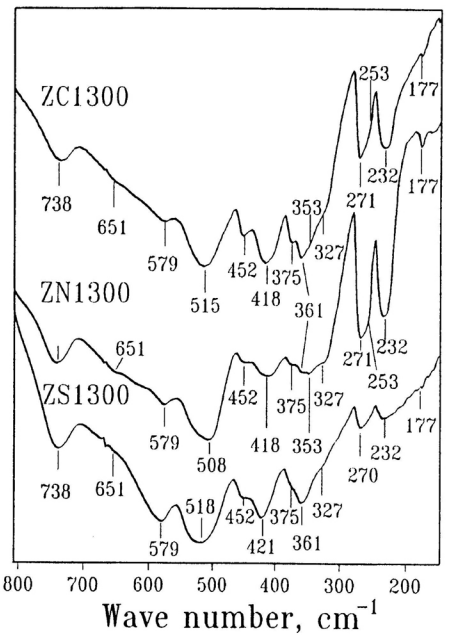

Figure 7. FT-IR spectra of samples: ZC1300, ZN1300 and ZS1300. The specimen for the FT-IR measurement was prepared by method (a), as described in Experimental.

FT-IR spectra of samples ZC1300, ZN1300 and ZS1300, shown in Figure 7, can be ascribed to m-ZrO_2.[28,30] Spectral differences are manifested for the main band, with a shift from 508 to 518 cm^{-1}. Also, the shoulder at 327 is most pronounced for sample ZN1300. The relative intensities of the bands at 271, 232 cm^{-1} and 177 cm^{-1} decreased in the order of the anion $NO_3^- \rightarrow Cl^- \rightarrow SO_4^{2-}$. Finally, the presence of a small amount of t-ZrO_2 in sample ZS1300 is probably due to a relatively stable sulfate anion that created the oxygen nonstoichiometry responsible for additional stabilization of t-ZrO_2 at very high temperature.

FT-IR spectra of the newly obtained sample ZC400 prepared for the measurement by methods (*a*) and (*b*), described in Experimental, are shown in Figure 8. Sample ZC400-A, prepared by method (*a*), shows a clear spectrum of the t-ZrO_2, with no evidence of bands characteristic of m-ZrO_2. Sample ZC400-B, prepared by method (*b*), shows bands typical of m-ZrO_2, with no evidence of the t-ZrO_2 bands.

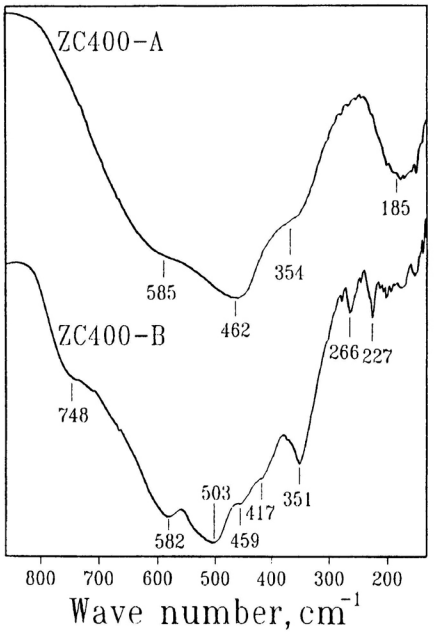

Figure 8. FT-IR spectra of samples: ZC400-A prepared from newly obtained sample ZC400 by method (a), as described in Experimental, and ZC400-B prepared from newly obtained sample ZC400 by method (b), as described in Experimental.

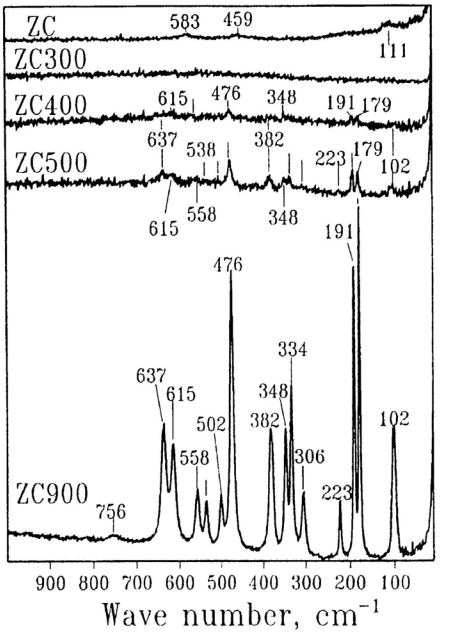

Figure 9. Laser Raman spectra of samples: ZC = $ZrOCl_2 \cdot 8H_2O$, ZC300, ZC400, ZC500 and ZC900. The specimen for the laser Raman measurement was prepared by method (c), as described in Experimental.

It is important to note that in the present investigation two new IR bands were observed that had not been reported in previous papers,[28–30] a very broad and strong band with transmittance minimum at 190 cm^{-1}, characteristic of *t*-ZrO_2, and another at ~177 cm^{-1} characteristic of *m*-ZrO_2 which is also Raman active.

Laser Raman spectroscopy

Results of the laser Raman spectroscopic measurements obtained with the samples prepared by method (*c*), described in the Experimental, are summarized in Figures 9, 10, 11 and 12. Figure 9 shows the laser Raman spectrum of $ZrOCl_2 \cdot 8H_2O$ and its thermal decomposition products. The characteristic peaks, observed for $ZrOCl_2 \cdot 8H_2O$, are located at 583, 459 and 111 cm^{-1}. The spectra of the sample ZC300 is »empty«; however, an increased background is observed in the region centered ~400-600 cm^{-1}. The

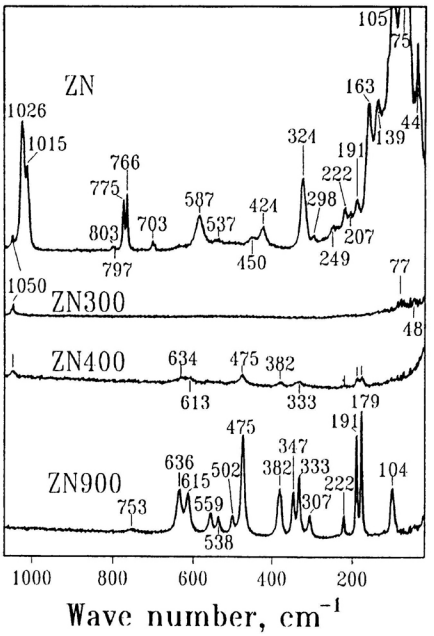

Figure 10. Laser Raman spectra of samples: ZN = $ZrO(NO_3)_2 \cdot 2H_2O$, ZN300, ZN400 and ZN900. The specimen for the laser Raman measurement was prepared by method (c), as described in Experimental.

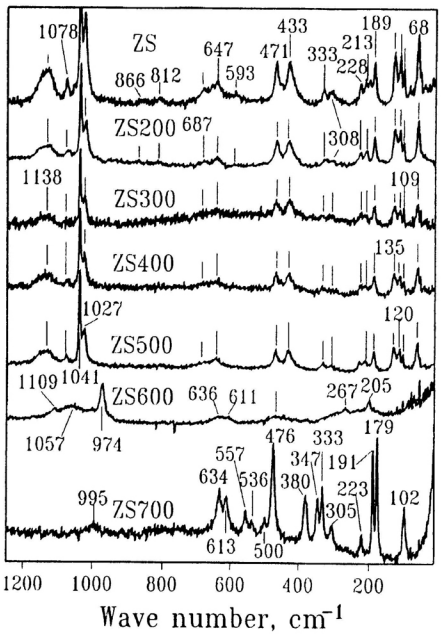

Figure 11. Laser Raman spectra of samples: ZS = $Zr(SO_4)_2 \cdot 4H_2O$, ZS200, ZS300, ZS400, ZS500, ZS600 and ZS700. The specimen for the laser Raman measurement was prepared by method (c), as described in Experimental.

ZC400 spectrum shows characteristic bands of m-ZrO_2 and no evidence of bands at 261 and 147 cm^{-1}, characteristic of t- ZrO_2.[14,30–33] These results were in controversy with the results obtained by XRD and also with the data available in literature.[4,9,25] It is evident that the sample underwent phase transition t-$ZrO_2 \rightarrow m$-ZrO_2. With a further increase of the heating temperature sharpening of the bands corresponding to m-ZrO_2 occurred. The spectrum of sample ZC900 can be ascribed to a well defined m-ZrO_2.[14,30,34] The Raman spectrum of sample ZC400, prepared by method (*d*), described in the Experimental, shows bands at 148 and 263 cm^{-1}, characteristic for t-ZrO_2, while no bands characteristic of m-ZrO_2 are observed. The background noise of the spectrum, similar to the case of the sample prepared by method (*c*), is very high, probably due to the florescence generated by the presence of Cl^- ions.

Figure 10 shows the laser Raman spectra of the $ZrO(NO_3)_2 \cdot 2H_2O$ and its thermal decomposition products, ZN300, ZN400 and ZN900. It is important to note that the spectrum of sample ZN300 does not show any peaks of either t-ZrO_2 and m-ZrO_2. The peaks at 1050, 77 and 48 cm^{-1} are due to

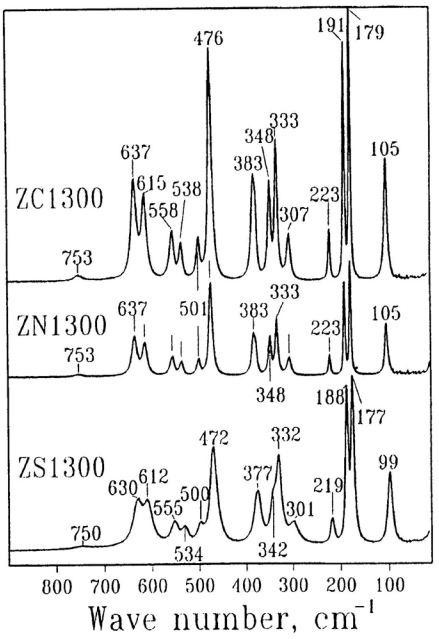

Figure 12. Laser Raman spectra of samples: ZC1300, ZN1300 and ZS1300. The specimen for the laser Raman measurement was prepared by method (a), as described in Experimental.

the undecomposed nitrate groups. Sample ZN400 shows weak bands characteristic of *m*-ZrO_2. Similarly, like in the case of ZC400, no presence of the *t*-ZrO_2 phase was detected, in spite of the fact that XRD showed approximately equal fractions of *m*-ZrO_2 and *t*-ZrO_2 in sample ZN400. Sample ZN900 showed a well defined spectrum of *m*-ZrO_2. The Raman spectrum of sample ZN400 prepared by method (*d*) shows bands characteristic of *m*-ZrO_2, and also the bands at 148 and 263 cm^{-1}, which can be ascribed to *t*-ZrO_2. Keramidas and White[14] used a method similar to our method (*c*) and the presence of the bands characteristic for *t*-ZrO_2, obtained in their work, indicated that metastable *t*-ZrO_2 was mechanically more stable than *t*-ZrO_2 prepared from zirconyl salts in our work.

Figure 11 shows the laser Raman spectra of $Zr(SO_4)_2 \cdot 4H_2O$ and its thermal decomposition products obtained up to 700 °C. The spectra of the samples obtained up to 500 °C exhibit the main features that are characteristic of the starting material, $Zr(SO_4)_2 \cdot 4H_2O$. In the region ~1000–1150 cm^{-1}, peaks characteristic of sulfate groups are well visible.[35,36] In the spectra of samples ZS600 and ZS700, bands at 974 and 995 cm^{-1} are formed. The presence of these Raman bands can be related to the sulfate groups. For instance, Choi *et al.*[37–39] investigated the Raman spectrum of Na_2SO_4 and observed two bands at 996,0 and 976,7 cm^{-1} respectively which were assigned to the ν_1(Ag) vibration mode in the sulfate group. The laser Raman spectrum of sample ZS600, besides the residual sulfates, also shows poorly resolved bands at 636–611 cm^{-1}, a very broad band centered at 476 cm^{-1}, as well as a very broad band with peaks at 267 and 205 cm^{-1}. Sample ZS700 also shows a peak at 267 cm^{-1} and also a small peak at 148 cm^{-1}. The appearance of these bands in samples ZS600 and ZS700 indicates the presence of the *t*-ZrO_2 phase in these samples.

Figure 12 shows the laser Raman spectra of samples ZC1300, ZN1300 and ZS1300. The spectra of sample ZC1300 and ZN1300 can be ascribed to a well defined m-ZrO_2. The spectrum of sample ZS1300 indicates shifting of the bands 637 → 630 and 615 → 612 cm^{-1}, 476 → 472 cm^{-1} and, instead of the band at 348 cm^{-1}, a shoulder at 342 cm^{-1} is formed. These changes are probably influenced by the oxygen nonstochiometry in m-ZrO_2 rather than by the presence of a small amount of the t-ZrO_2 phase, as detected by XRD.

CONCLUSION

The fact observed in the present work that all three different zirconium salts give the same broad bands at 450 cm^{-1} in the corresponding FT-IR spectra may be an indication that the transition from zirconium salts to zirconium dioxide proceeds through a structurally similar intermediary. This is supported by the fact that all salts show the existence of metastable t-ZrO_2, which disappeared with further thermal treatment. The t-ZrO_2 to m-ZrO_2 ratios, measured by XRD, were dependent on the nature of the starting salt. Having in mind the different fractions of t-ZrO_2 and m-ZrO_2 in samples, obtained after the heating of $ZrOCl_2 \cdot 8H_2O$ and $ZrO(NO_3)_2 \cdot 2H_2O$ up to 400 °C, it may be concluded that the structural parameters of $ZrOCl_2 \cdot 8H_2O$ were closer to t-ZrO_2 than those of $ZrO(NO_3)_2 \cdot 2H_2O$. This conclusion may be supported by the similarities of FT-IR spectra of $ZrOCl_2 \cdot 8H_2O$ and sample ZC400, which was almost pure t-ZrO_2. Further increase of heating temperature showed that t-ZrO_2 formed from $ZrOCl_2 \cdot 8H_2O$ was thermally most unstable, while the presence of t-ZrO_2 formed from $Zr(SO_4)_2 \cdot 4H_2O$ was noticed even at a temperature of 1300 °C. Metastable t-ZrO_2 obtained by the thermal decomposition of $ZrOCl_2 \cdot 8H_2O$ and $ZrO(NO_3)_2 \cdot 2H_2O$ showed a very high sensitivity to mechanical treatment, while metastable t-ZrO_2 formed from $Zr(SO_4)_2 \cdot 4H_2O$ was stable during the same process. Finally, it may be concluded that the formation of metastable t-ZrO_2 was mostly influenced by the nature of the starting salt but, once t-ZrO_2 was formed, its stability depended on the anionic impurities that remained in the oxide material.

Acknowledgment. – The authors greatefully acknowledge the support of the USA (National Institute of Standards and Technology) – Croatia (Ministry of Science and Technology) Joint Fund (grant No JF106).

REFERENCES

1. C. J. Howard, R. J. Hill, B. E. Reichert, *Acta Cryst.* **B44** (1988) 116.
2. International Centre for Diffraction Data, Newtown Square, Pa 19073-3273, U.S.A., Powder Diffraction File.
3. G. Teufer, *Acta Cryst.* **15** (1962) 1187.

4. I. Clark and D. H. Reynolds, *Ind. Eng. Chem.* **29** (1937) 711.
5. R. C. Garvie, *J. Phys. Chem.* **69** (1965) 1238.
6. R. C. Garvie, *J. Phys. Chem.* **82** (1978) 218.
7. E. Bailey, D. Lewis, Z. M. Librant and L. J. Porter, *Trans. J. Br. Ceram. Soc.* **71** (1972) 25.
8. A. Mumpton and R. Roy, *J. Am. Ceram Soc.* **43** (1960) 234.
9. D. Whitney, *Trans. Faraday Soc.* **61** (1965) 1991.
10. R. Cypres, R. Wollast and J. Raucq, *Ber. Dtsch. Keram. Ges.* **40** (1963) 527.
11. A. Clearfield, *Inorg. Chem.* **3** (1964) 146.
12. T. Mitsuhasi, M. Ichihara and U. Tatsuke, *J. Am. Ceram Soc.* **57** (1974) 97.
13. J. Livage, K. Doi and C. Mazieres, *J. Am. Ceram. Soc.* **51** (1968) 349.
14. G. Keramidas and W. B. White, *J. Am. Ceram Soc.* **57** (1974) 22.
15. E. Tani, M. Yoshimura and S. Somiya, *J. Am. Ceram Soc.* **66** (1983) 116.
16. Y. Murase and E. Kato, *J. Am. Ceram Soc.* **66** (1983) 196.
17. T. Sato, F. Ozawa, T. Nakamura, H. Watanabe and S. Ikoma, *Thermochim. Acta* **34** (1979) 211.
18. Y. Murase and E. Kato, *J. Am. Ceram Soc.*, **62** (1979) 527.
19. B H. Davis, *J. Am. Ceram Soc.* **67** (1984) C-168.
20. R. Srinivasan, L. Rice and B. H. Davis, *J. Am. Ceram Soc.* **73** (1990) 3528.
21. R. Srinivasan, B. H. Davis, O. Burl Cavin and C. R. Hubbard, *J. Am. Ceram Soc.* **75** (1992) 1217.
22. T. Mamott, P. Barnes, S. E. Tarling, S. L. Jones and C. I. Norman, *J. Mater. Sci.*, **26** (1991) 4054.
23. J. Torralvo, M. A. Alario and J. Soria, *J. Catal.* **86** (1984) 473.
24. I. Osendi, I. S. Moya, C. I. Serna and I. Soria, *J. Am. Ceram Soc.* **68** (1985) 135.
25. R. Ravelle-Chapuis, M. G. Blanchin, M. Jerbrouni, B. Durand, *Euro-ceramics* **2** (1989) 2.97
26. H. Toraya, M. Yoshimura, S. Somiya, , *J. Am. Ceram Soc.* **67** (1984) C119.
27. H. P. Klug, L. E. Alexander: *X-ray Diffraction Procedures*, 2nd edition, John Wiley & Sons, New York 1974., pp. 640-642, (Fig. 9.9).
28. N. T. McDevitt and W. L. Baun, , *J. Am. Ceram Soc.* **47** (1964) 622.
29. D. M. Lui, C. H. Perry and R. P. Ingel, *J. Appl. Phys.* **64** (1988) 1415.
30. C. M. Phillippi and K. S. Mazdiyasni, *J. Am. Ceram Soc.* **54** (1971) 254.
31. H. Arashi and M. Ishigame, *Phys. Stat. Sol.* **71** (1982) 313.
32. D. J. Kim, H. Jung and I. S. Yang, *J. Am. Ceram Soc.* **76** (1993) 2106.
33. M. Yashima, H. Arashi, M. Kakihana and M. Yoshimura, *J. Am. Ceram Soc.* **77** (1994) 1067.
34. C. H. Perry, F. Lu, D. W. Liu and B. Alzyab, *J. Raman Spec.* **21** (1990) 577.
35. S. Musić, S. Popović, Z. Orehovec and I. Czakó-Nagy *J. Coll. Interface Sci.* **160** (1993) 479.
36. S. Musić, Z. Orehovec, S. Popović and I. Czakó-Nagy, *J. Mater. Sci.* **29** (1994) 1991.
37. B.-K. Choi and D. J. Lockwood, *Solid State Comm* **72** (1989) 133.
38. B.-K. Choi and D. J. Lockwood, *Solid State Comm* **74** (1990) 109.
39. B.-K. Choi and D. J. Lockwood, *Solid State Comm* **76** (1990) 863.

SAŽETAK

Stvaranje ZrO_2 termičkom razgradnjom cirkonijevih soli

Goran Štefanić, Svetozar Musić, Stanko Popović i Krešimir Furić

Hidratizirane cirkonijeve soli, koje su sadržale anione Cl^-, NO_3^- ili SO_4^{2-}, grijane su do 1300 °C. Produkti termičke razgradnje istraživani su difrakcijom X-zraka, FT-IR spektroskopijom i laserskom Ramanovom spektroskopijom. Amorfni materijal, dobiven termičkom razgradnjom svih triju cirkonijevih soli, pokazao je maksimum raspršenja X-zraka pri ~16° te široku vrpcu u FTIR spektru pri 450 cm^{-1}. S povećanjem temperature sve tri soli (400 °C za $ZrOCl_2 \cdot 8H_2O$, 400 °C za $ZrO(NO_3)_2 \cdot 2H_2O$ i 700 °C za $Zr(SO_4)_2 \cdot 4H_2O$) su dale metastabilni *t*-ZrO_2, koji je nestao s daljnjim povećanjem temperature. Rezultati su pokazali da se prijelaz iz cirkonijevih soli u cirkonijev dioksid odvija preko strukturno sličnih međufaza sa strukturnim parametrima koji pogoduju nastanku *t*-ZrO_2. Udjeli *t*-ZrO_2 i *m*-ZrO_2 određeni difrakcijom X-zraka ovisili su o prirodi cirkonijeve soli. Zaključeno je da su strukturni parametri soli $ZrOCl_2 \cdot 8H_2O$ bliži *t*-ZrO_2, nego što je slučaj sa soli $ZrO(NO_3)_2 \cdot 2H_2O$. Faza *t*-ZrO_2 dobivena iz $ZrOCl_2 \cdot 8H_2O$ bila je termički najnestabilnija, za razliku od *t*-ZrO_2 faze dobivene iz $Zr(SO_4)_2 \cdot 4H_2O$ prisutnost koje je registrirana i u uzorku dobivenom nakon žarenja pri 1300 °C. Može se zaključiti da udjel nastaloga metastabilnog *t*-ZrO_2 ovisi o prirodi ishodnih soli, međutim, kad je jednom stvoren *t*-ZrO_2, njegova daljnja stabilnost ovisi o anionskim primjesama zaostalima u oksidnom materijalu.